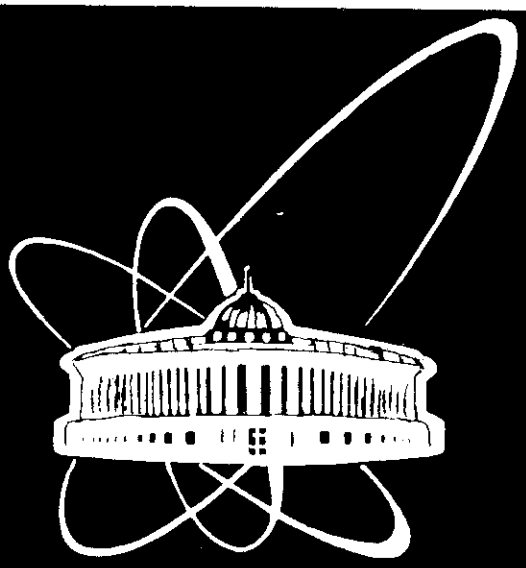

СООБЩЕНИЯ
ОБЪЕДИНЕННОГО
ИНСТИТУТА
ЯДЕРНЫХ
ИССЛЕДОВАНИЙ

Дубна

E E

E7-99-240

CERN LIBRARIES, GENEVA
SCAN-0003044

WIDE APERTURE MULTIPOLE MAGNETS OF THE KINEMATIC SEPARATOR **COMBAS**

Analyzing Multipole Magnets M2 and M7 with Compensation for Higher Order Aberrations

1999

A.G.Artukh, G.F.Gridnev, Yu.G.Teterev
Joint Institute for Nuclear Research, 141980, Dubna, Russia

M.Grushezki, F.Koscielniak, J.Szmider
Henryk Niewodniczanski Institute for Nuclear Physics, Crakow, Poland

A.G.Semchenkov*, O.V.Semchenkova, Y.M.Sereda, I.N.Vishnevski
Institute for Nuclear Research, Kiev, Ukraine

V.A.Shchepunov
Laboratorio Nazionale del Sud INFN, 95123 Catania, Italy

Yu.P.Severgin, V.V.Koreniuk, E.A.Lamzin, M.G.Nagaenko, S.E.Sytchevski
Efremov Scientific Research Institute of Electrophysical Apparatus, St. Petersburg, Russia

*E-mail: semchenkov@main1.jinr.ru

© Объединенный институт ядерных исследований. Дубна, 1999

1. Introduction

An essential element of any separating system, based on the separation with magnetic field, is a bending magnet that performs the main momentum analyzing function. Beam focusing and higher order corrections are performed by introducing quadrupole, sextupole, octupole etc field components in the magnetic structure of a device. In the kinematic separator COMBAS quadrupole and higher order field components have been introduced in the main dipole fields of the separator magnets. Such an approach allowed one to exclude separate focusing quadrupoles and correcting sextupoles and octupoles, increase angular and momentum acceptances of the device and shorten its total length [1-3]. Analyzing magnets M2 and M7 (12X55ECH164-1.125-25, see Fig.1) were calculated, designed and manufactured as a part of the separator that consists of 8 combined functions magnets M1-M8.

One should note that the magnet M2 together with M1 make up the analyzing section of the fragment-separator (see Fig.2 in [3]) and, in the linear approximation, completely determine the system's optical properties. Magnet M1 focuses in the vertical plane and defocuses in the horizontal plane. The action of magnet M2 on the beam is reverse. The 1st order field indexes of M1 and M2 are opposite in sign. The use of such a magnetic structure let, flexibly and efficiently, form a beam of required profile and size and, in addition, to facilitate the minimization for the higher order spherical aberrations, which increase considerably the image size in wide aperture magnetic systems.

2. The main technical characteristics of the magnets

Main stages of the design and manufacturing of the magnets M2, M7 have been described in [3]. M2 and M7 (see Fig.2) have 4 m bending radius, 25deg deflection angle and the weight of 27 tons each. The 1st order field index n=-6.75, sextupole and octupole field components are non zero and, hence, the vertical gap size varies with radius. The gap size is as large as 100 mm in the central ray region (**dR**=0 mm), 50 mm in the region of the maximum radius (**dR**=400 mm) and more than 300 mm at the minimum radius (**dR**=-400 mm). The pole pieces have been profiled to obtain required field components. It is the design and manufacturing of the pole pieces that became the most challenging. The four magnet poles were produced from a single piece of an iron blank. A special merry-go-round machine, whose rotatable section's diameter was as large as 10 m, has been used. This let produce pole pieces having identical shape and magnetic properties.

The main technical parameters of the magnets M2 (M7) are given in the Table.1.

3. Measurements of the magnetic characteristics

3.1. Magnetic measurements

The magnetization curve and the field distributions in the median plane of M2, M7 for three levels of the induction $\mathbf{B_0}$=7300, 9800, 11610 Gs (I=500, 705, 905 amps., respectively) have been measured in the FLNR JINR (Dubna). Three-component field distributions have also been measured, for the same three induction levels, on the surface of a closed volume between pole pieces.

To carry out three-component measurements of the magnetic fields in M2, M7 a computer-based measurement system has been designed and built (see Fig.3). The system consists of:

- two heads (see Fig.3 c)) in [4]) for measurements of $\mathbf{B_x}$, $\mathbf{B_y}$ and $\mathbf{B_z}$, each head consisting of three Hall probes (having dimensions 2*2*0.1 mm) located at distances 10 mm from each other along the axis **OX**. The probe positioning accuracy within the measuring head was 0.1 mm. A special bench has been used to calibrate the angle of rotation of the probes around the axes **OZ**, **OY** and **OX** (this was not more than 2 degrees). The field components reciprocal dependencies were taken into account in the final build of the magnetic field map,
- two monitoring probes for monitoring the temperature and time stability during the prolonged magnetic measurements. The probes were placed in a narrow part of the gap with a high magnetic field of more than 10kGs. The probes' readouts have been used to normalize the results of the magnetic measurements,
- measuring carriage equipped with two separable plates with holes, enabling the heads to be installed with the accuracy of 0.1 mm,
- a guide (attached to the neutral pole of the magnet), which enabled moving the measuring carriage with probes along the gap (in the beam direction). From the opposite side of the magnet the measurement carriage was supported from the lower pole,
- an electrical drive including a stepper (a step motor SHD-5) and a belt of stainless steel moving the measuring carriage along the guide with the accuracy of 0.02 mm (step of the motor) along the axis **X**,
- a control unit for the power supply of the stepping motor with a control card in an IBM PC,
- a measurement channel for the Hall probes' currents built on the basis of the precision digital voltmeter SOLARTON (the voltage measurement accuracy is 1 mkV) having a digital outlet and the SOLARTRON 7010 MINATE commutator,

- a computer control program for controlling the stepper, the eight-channel system for the readout of the measured data from the digital voltmeter and writing the data on the IBM PC hard disc according to the standard RS-232.

A cartesian coordinate system has been used in the measurements having
- **OX** axis tangential to the magnet radius at the magnet central point (0,0,0),
- **OY** axis directed towards the greater radius at the magnet central point,
- **OZ** axis directed down according to the positive value of the induction.

Along the axis **OX** the measuring head moved automatically with a step of 20mrad, while its positioning along the axes **OY** and **OZ** was done manually with steps 20 mm and 5 mm respectively. The field was measured in the following ranges: ± 0.25rad along the axis **OX**, ± 400 mm along the axis **OY** and $\pm 20/\pm 40$ mm along the axis **OZ** depending on the vertical gap size.

Field components at each point were measured repeatedly 5 times. The r.m.s. measurement error due to the head positioning errors (caused by the head assembling and stepper positioning errors) and errors of measuring the voltage was not more than 2 Gauss, or 0.02% of the field in the center of the magnet.

The magnetic field was measured on the closed surface that included:
- the surfaces along the upper and lower poles,
- the left and right lateral surfaces,
- the surfaces at the smallest and largest radii,
- the median plane.

A sketchy view of the measurement planes (in the section **YOZ**) is shown in the Fig.4. The measurement planes near the surface of the pole pieces were chosen according to the size of the vacuum chamber and the gap. Namely, in the region of

small gap sizes there was a problem of approaching the probes as close as possible to the pole pieces, while in the region of larger gaps we contented with the area confined by the vacuum chamber.

The magnetic measurements were organized as follows. First, the field was measured in the median plane. This was done in two steps: in the region from the magnet entrance till the center of the magnet and then from its exit till the center. The measured grid for each half of the median plane contained 42 points in the radial direction and 62 points in the beam direction. To match these two sets of measured data between themselves they had common measured points in the center of the magnet. The total number of the grid points, excluding the repeated ones, was approximately 5000. The fields in the horizontal planes near the lower and upper pole pieces (see Fig. 4) have been measured similarly with the total number of the grid points of about 6000 for each pole piece. Then the field in two vertical planes, at the minimum and maximum radii (1 and 6 in Fig. 4), has been measured in 2000 and 1000 points respectively. Finally, the measurements in the lateral planes (at the magnet entrance and exit) have been done with the carriage fixed with special pawls. More than 630 points have been measured in each plane. Thus, the total number of the measured points was more than 21000 per one induction level. These measurements have been done for 3 induction levels mentioned above in 3.1.

3.2. The magnetization curve

The magnetization curve measured in the center of the magnet M2 is shown in the Fig. 5 (circles) in comparison with simulated points (squares). The measured points lie above the calculated one. For example, for the current I=650 amps. such a difference is as large as 500 Gs (5.7 %).

3.3. Analysis of the field distribution in the central section

The induction distributions of the magnets M2 and M7 were analyzed with the procedure described in [3]. The measurements displayed that the difference between induction values in M2 and M7 did not exceed 0.2%. Therefore, it's possible to draw a conclusion about the practical identity of M2 and M7.

As one can see quadrupole, sextupole and octupole components are presented in the distribution. Namely, the quadrupole component shows itself as a linear increase of the field from smaller to larger radii. (Respectively, the gap decreases from smaller to larger radii.) The sextupole and octupole components contributions are seen as deviations of the behavior of the curve from the linear low at minimum and maximum radii.

Analysis of the measurement data displayed that the deviation of the measured values from the calculated ones was, within the working area of the magnets of $\pm$ 400mm, not more than 2.0% for the all three field levels $\mathbf{B_0}$=7200, 9900 and 11600 Gs. In the smaller range of $\pm$ 350 mm this error did not exceed 1% for the all field levels. The mentioned error of 2.0% takes place in the area of larger radii (the smaller gaps and higher inductions), where the saturation is noticeable. The saturation results in the reduction of the radial working width down to $\pm$ 350 mm (about 90% of the nominal width) for magnetic rigidities higher than 4.0 T*m.

3.4. An analysis of the field distribution in the median plane

The procedure of the analysis of the median plane field has been described in [3].

The distribution of the $\mathbf{B_z}$-component in the median plane is shown Fig.6 for the field level $\mathbf{B_0}$=11600Gs ($\mathbf{B_x}$ and $\mathbf{B_y}$-components in the median plane are equal to zero). The field distribution along the axis **OY** at **X**=0 is the one presented in the Fig.7. The positive value of $\mathbf{B_z}$ corresponds to the direction downward. Analysis of the measured data showed that the effective lengths of both the magnets at the all field levels $\mathbf{B_0}$=7200, 9900 and 11610 Gs are greater than the nominal one, exceeding slightly the design tolerance. This can be compensated for by proper reductions of the induction values to provide the nominal deflection angle of 25 deg.

3.5. The field distribution near the lower pole

One of the main purposes of the tree-component magnetic field measurements was that of obtaining **3D** magnetic field maps of the all magnets, in part M2 and M7, to be used subsequently for the computerized particle raytracing through the entire separator. For this we have measured the $\mathbf{B_x}$-, $\mathbf{B_y}$- and $\mathbf{B_z}$-components of the magnetic fields in the closed surface described above. In this section the measurements of the $\mathbf{B_x}$- and $\mathbf{B_z}$-components near the lower pole piece are presented.

Fig. 8 represents the measured component $\mathbf{B_x}$ of the field in the 5 planes situated near the lower pole of M2 at distances -45, -40, -35, -30 and -25 mm from the median plane (see 8 in Fig.4) for the field level B_0=7050 Gauss. The component $\mathbf{B_x}$ is the projection of the magnetic field vector on the unit vector tangential to the optical axis of M2. The evolution of $\mathbf{B_x}$ along the axis **OX,** typical for any dipole magnet, can be understood easily from Fig.9 a) showing schematically the **XOZ** section of M2. As the coordinate X changes from big negative to big positive values passing through the magnet the component $\mathbf{B_x}$ subsequently grows, reaches its maximum positive value in the vicinity of the effective field boundary, decreases and passes zero

value in the center of the magnet, and then repeats the same evolution but in the opposite order and with the opposite sign.

One can see from Fig.8 that the absolute values of the $\mathbf{B_x}$ maximums (minimums) near the entrance (exit) EFB's are bigger at bigger **Y** values. This is due to smaller gap sizes and, hence, higher magnetic flux densities in the area of larger **Y**. One can see also sharp jumps in the dependence of $\mathbf{B_x}$ on **Y**, which are due to the fact that the component was measured in the 5 different planes, mentioned above, situated at different distances from the median plane.

Fig.10 presents the measured distribution of the component $\mathbf{B_z}$ in the planes near lower pole of M2 for the field level $\mathbf{B_0}$=7050 Gauss. The character of the distribution in the central section repeats that for the median plane (see Fig.6). As compared with the behavior of $\mathbf{B_z}$ in the median plane (see Fig.7), the values of $\mathbf{B_z}$ in this distribution drop faster from its maximum values to zero when the effective field boundaries are crossed.

4. Conclusion

The performed measurements of the fields in the magnets M2 and M7 of the fragment separator COMBAS showed satisfactory design and manufacturing quality. In part, the field distributions are quite symmetrical. No any shells or domains with anomalous magnetization have been discovered as a result of careful inspections of the distributions. The fields of M2 and M7 are practically identical: differences in the induction values in the median plane are less than 0.2%, and in the effective lengths less than 0.05%.

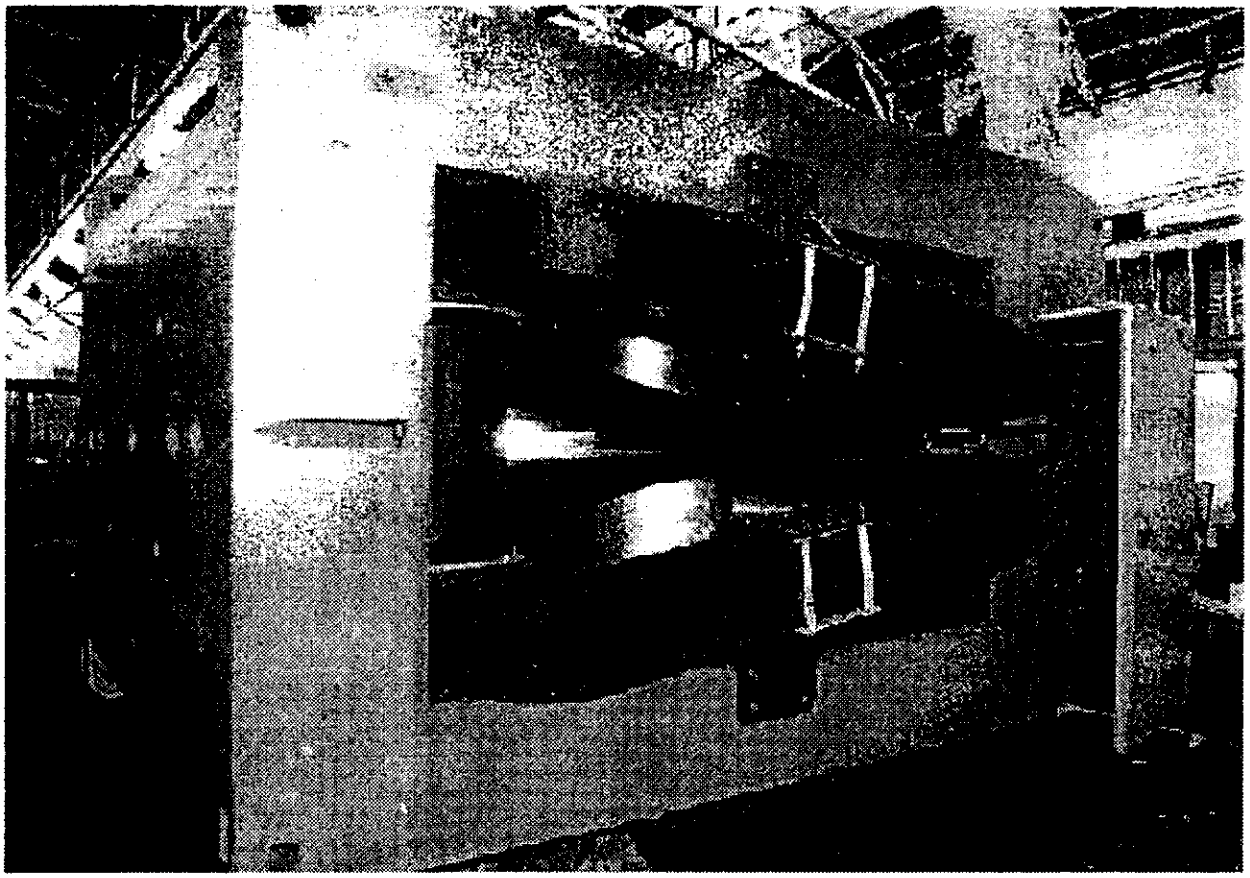

Fig.1. Analyzing multipole magnet M2 (12X55ECH164-1.125-25).

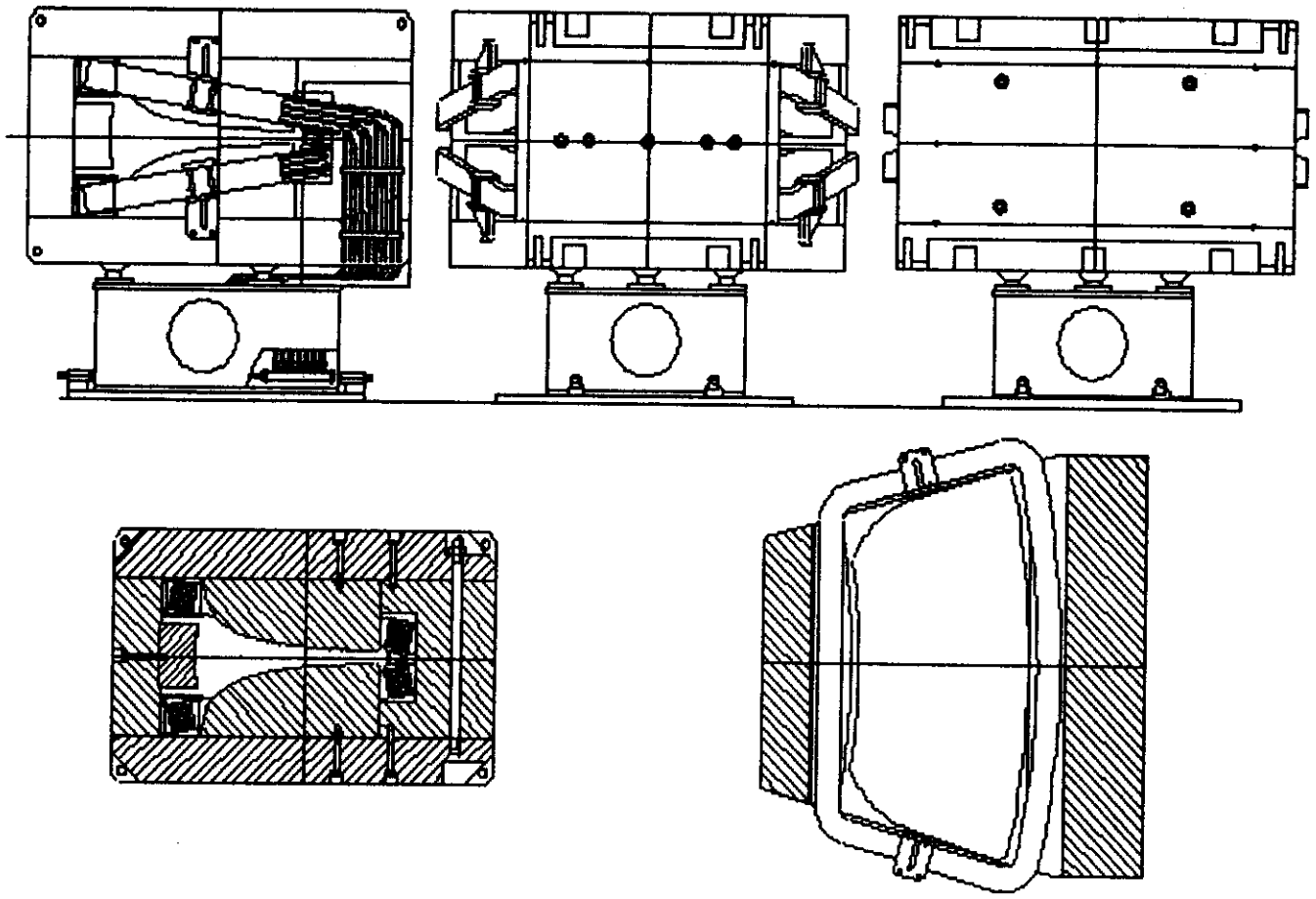

Fig.2. The drawing and sections of multipole magnets M2, M7.

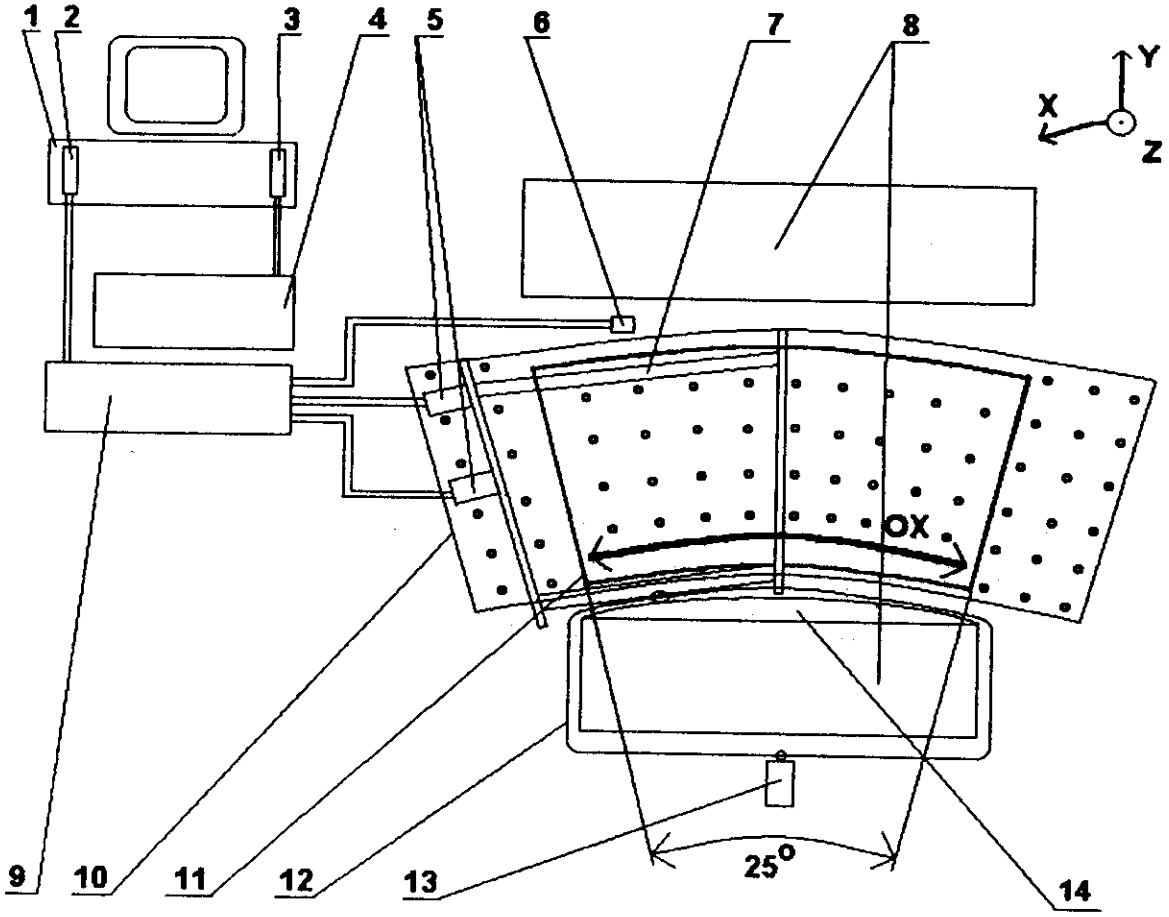

Fig.3. Block diagram of the automated system for the magnetic field measurements of the magnets M2 and M7. Figure denotes:

1- the control computer IBM PC AT (486);
2- the controller for connection with the SOLARTRON digital voltmeter;
3- the controller for the power supply assemblies of the **X**-coordinate displacement stepper;
4- the power supply module for the **X**-coordinate displacement stepper;
5- two measuring heads having 3 Hall probes each;
6- the monitoring Hall probes;
7- the measuring carriage;
8- the magnet M2 (M7);
9- the SOLARTRON precision digital voltmeter;
10- the magnetic field measurement area;
11- the area within effective field boundaries (deflection angle 25 deg, central radius $\mathbf{R}_0$=4m);
12- the **X**-coordinate displacement belt drive;
13- the **X**-coordinate displacement stepper;
14- the neutral pole of the magnet.

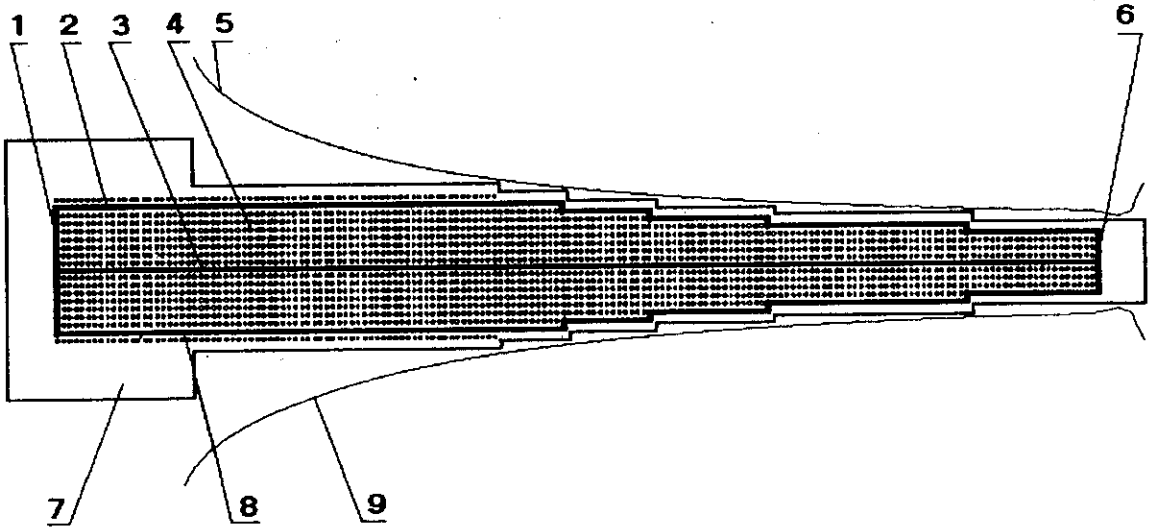

Fig.4. The measurement planes and points (vertical section **YOZ**):

1- the measurement plane at the minimum radius,

2- the measurement plane along the upper pole of the magnet,

3- the median plane,

4- the points of measurements in the lateral planes,

5- the upper pole surface of the magnet,

6- the measurement plane at the maximum radius,

7- the measuring carriage plate,

8- the measurement plane along the lower pole of the magnet,

9- the lower pole surface of the magnet.

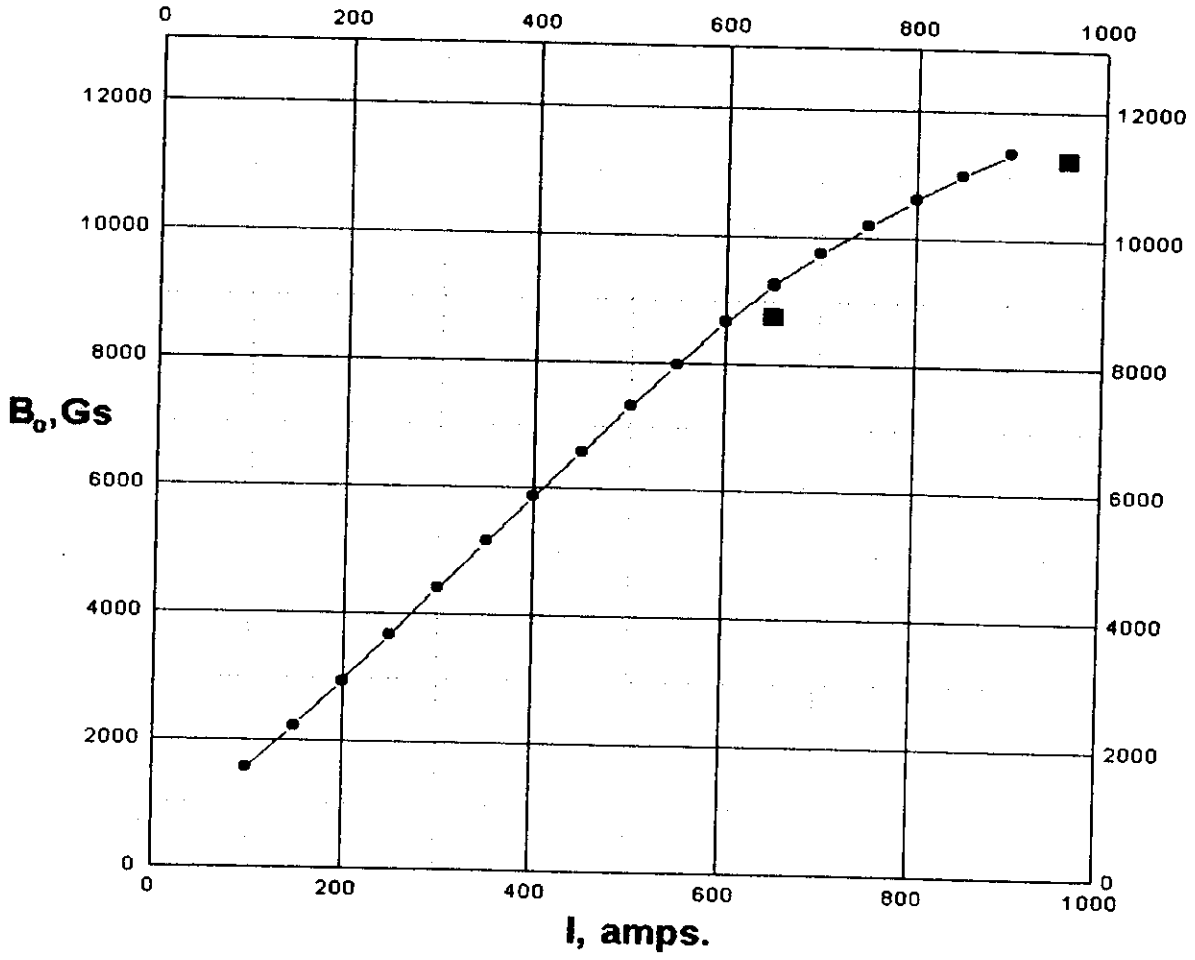

Fig.5. The magnetization curve of the magnet M2: the squares represent theoretical calculations, circles – experimental data.

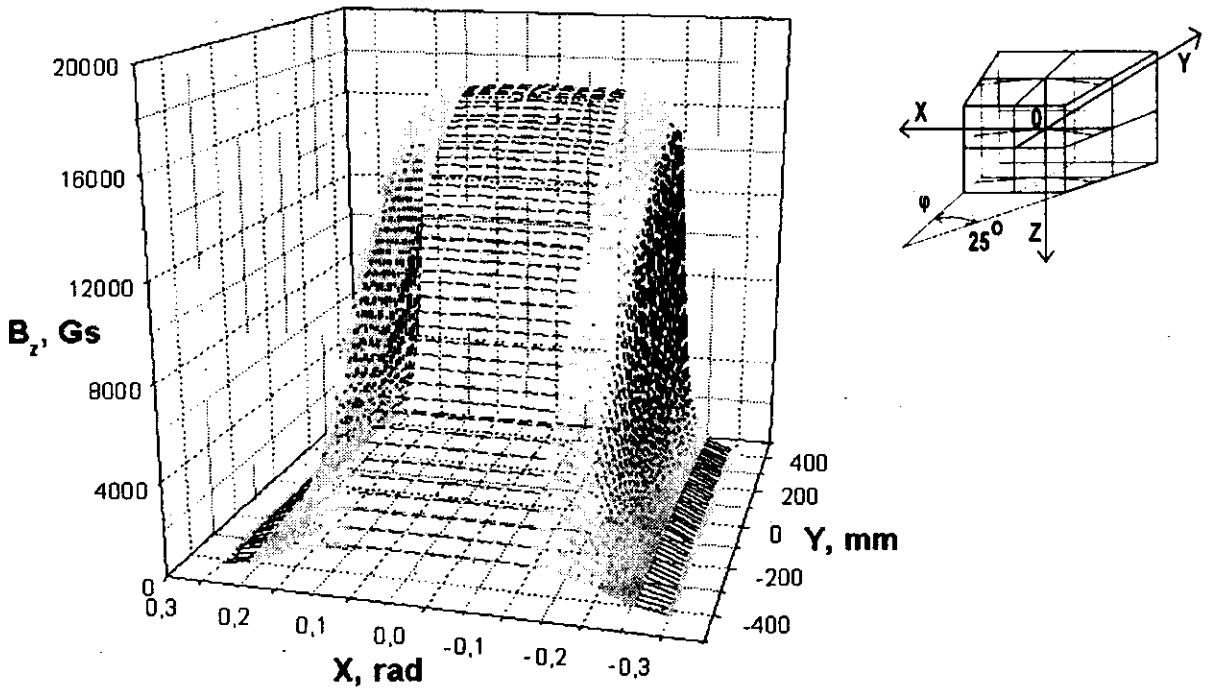

Fig.6. The measured distribution of the B_z-component of the magnetic field in the median plane of M2.

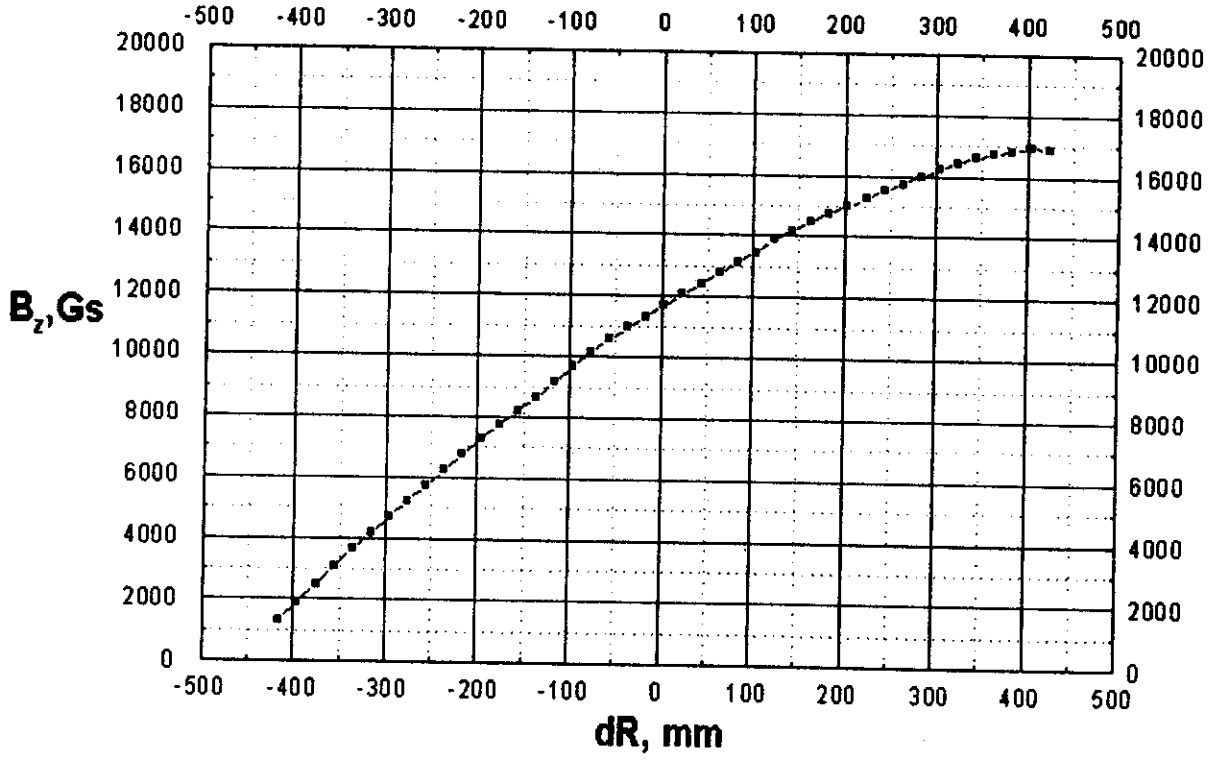

Fig.7. The magnetic field distribution in the central section of the magnet M2 for the field level $\mathbf{B_0}$=11600 Gauss. The measured points coincide with the values, calculated according to the equations (3) and (4) [3], with the accuracy better than 2.0%.

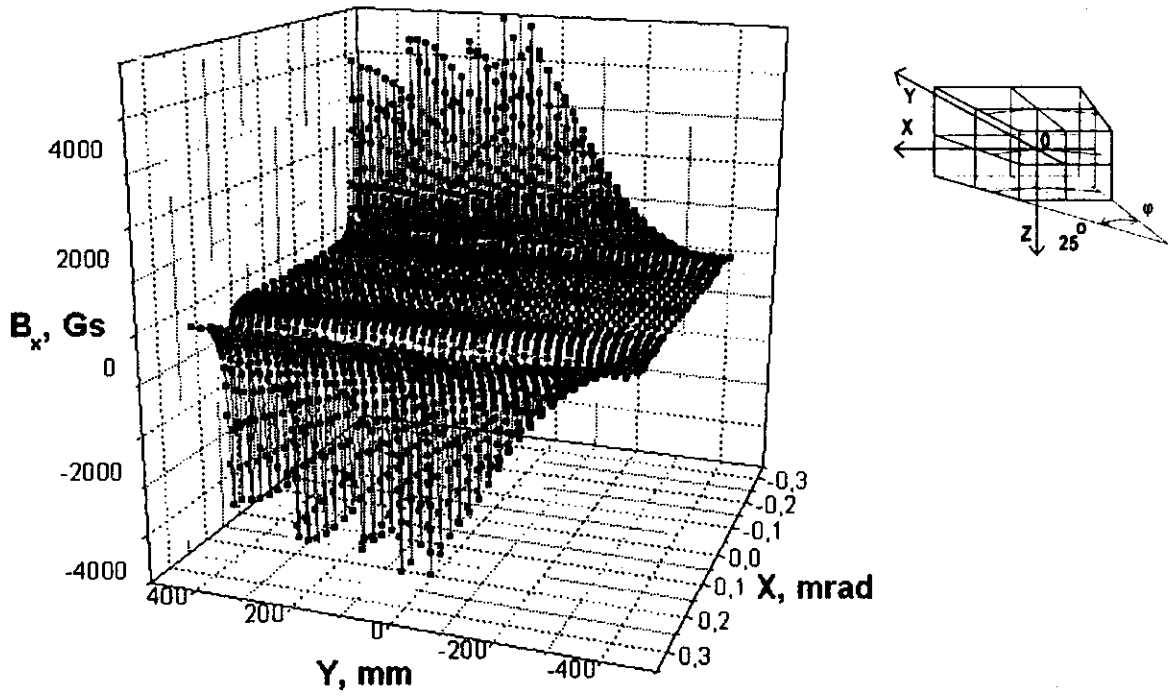

Fig.8. The measured distribution of the component $\mathbf{B_x}$ of the magnetic field near the lower pole of M2 at distances –45, -40, -35, -30 and –25 mm from the median plane.

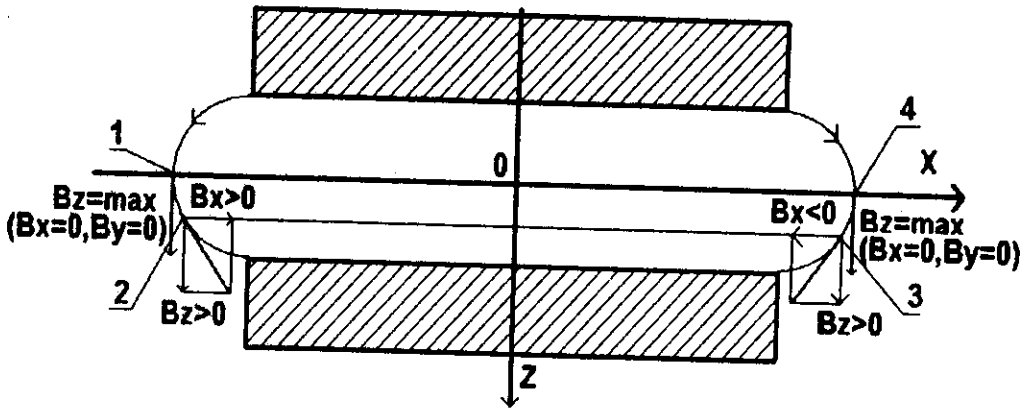

a)

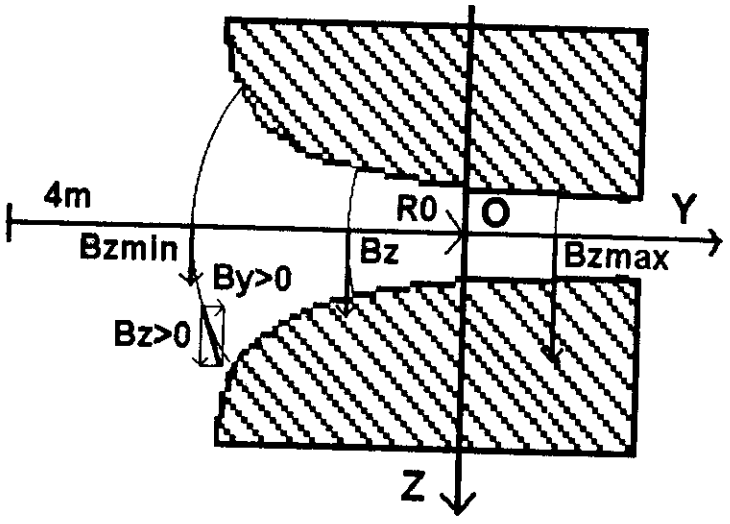

b)

Fig.9. The sketchy image of the vertical sections of the magnet M2 in the measurement planes **XOZ** (a) and **YOZ** (b). The axes **OX** in the figure a) and **OY** in b) lie in the median plane. Field lines going from the upper to the lower pole are shown. The directions of the magnetic field vector are indicated with arrows in the points 1-4, points 1,4 belonging to the median plane and 2, 3 to the plane situated near the lower pole.

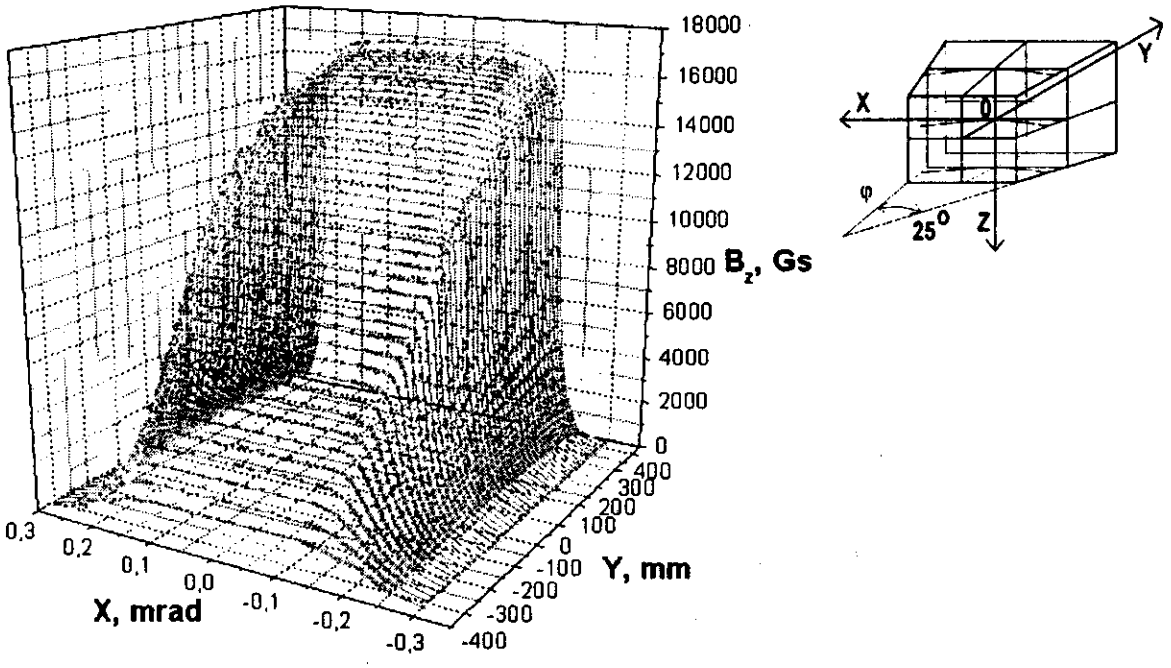

Fig.10. The measured distribution of the component $\mathbf{B}_z$ near the lower pole of M2.

Table 1.

Basic parameters of the magnets M2-M7.

Parameters	Values
Maximum induction on the central trajectory (T)	1.125
Nominal induction on the central trajectory(T)	0.875
Radius of the central trajectory (m)	4
Working width of the pole pieces (mm)	800(±400)
Gap along the central trajrctory (mm)	100
Effective length (mm)	1746
Deflection angle (deg)	25
Resistanse of coils (Ω)	0.07
Maximal current (amps.)	960
Rated current (amps.)	650
Maximal Voltage (v)	68
Rated Voltage (v)	48
Maximal Power (kwatt)	65
Rated Power (kwatt)	31.2
Inductance of coils (H)	0.3
Water discharge (liter per minute)	28
Water overheading (C)	40
Copper mass (tns)	1.0
Steel mass (tns)	25
Total magnet mass (tns)	27

The obtained data let us build three-components field maps for three induction levels. These maps will be used for particle raytracing throughout the entire apparatus.

5. Acknowledgments

The authors are indebted to Yu.Ts.Oganesian, V.Z.Majdikov for the fruitful discussions and support. We appreciate A.A.Alexeeva for the manuscript preparation.

6. References

1. A.G.Artukh et al., Nucl. Instr. and Meth. A 306 (1991) 123.
2. A.G.Artukh et al., Nucl. Instr. and Meth. A 426 (1999) 605.
3. A.G.Artukh et al., Commun. JINR E7-99-238, Dubna, 1999.
4. A.G.Artukh et al., Commun. JINR E7-99-239, Dubna, 1999.

Received by Publishing Department
on September 9, 1999.

Артюх А.Г. и др.
E7-99-240

Широкоапертурные мультипольные магниты кинематического сепаратора КОМБАС.
Анализирующие мультипольные магниты М2 и М7 с компенсацией аберраций высоких порядков

Создан и введен в эксплуатацию высокоразрешающий широкоапертурный кинематический сепаратор КОМБАС, магнитная структура которого выполнена на принципе жесткой фокусировки. Сепаратор состоит из восьми широкоапертурных мультипольных магнитов М1—М8. В состав сепаратора вошли поворотные мультипольные магниты М2 и М7 с введенными в распределение поля квадрупольной, секступольной и октупольной компонентами. Наличие данных компонентов позволило отказаться от квадрупольных линз, а также добиться минимизации сферических аберраций и компенсации хроматических эффектов. Для магнитов М2 и М7 проведены трехкомпонентные магнитные измерения по замкнутому объему, позволившие проанализировать качество их изготовления. По данным измерений предполагается составить трехмерные карты магнитного поля. Карты полей магнитов будут использованы для проведения траекторных расчетов по трассировке частиц через сепаратор.

Работа выполнена в Лаборатории ядерных реакций им. Г.Н.Флерова ОИЯИ.

Сообщение Объединенного института ядерных исследований. Дубна, 1999

Artukh A.G. et al.
E7-99-240

Wide Aperture Multipole Magnets of the Kinematic Separator COMBAS.
Analyzing Multipole Magnets M2 and M7 with Compensation for Higher Order Aberrations

The high-resolving large aperture kinematic separator COMBAS has been created and commissioned. The magneto-optical structure of separator is based on the strong focusing principle. The separator consists of eight wide aperture multipole magnets M1—M8. In part, the separator includes bending multipole magnets M2 and M7 having quadrupole, sextupole and octupole components in their field distributions. The presence of these components allowed one to intensify focusing without separate quadrupoles, minimize spherical aberrations and compensate for chromatic effects. Three-component magnetic field measurements on the surface of a closed volume have been performed for the magnets M2 and M7. These measurements allowed one to analyze the magnet manufacturing quality. The measured data will allow compile 3D-maps of magnetic fields. The 3D-maps of the magnetic field is supposed to be used for the particle trajectory simulations throughout the separator.

The investigation has been performed at the Flerov Laboratory of Nuclear Reactions, JINR.

Communication of the Joint Institute for Nuclear Research. Dubna, 1999